Chapter 7

The Effect of Alloy Microstructure on Their Cavitation Erosion Behavior in Seawater

Abdulhameed Al-Hashem,
Abdulmajeed Abdullah and Wafa Riad

Additional information is available at the end of the chapter

http://dx.doi.org/10.5772/intechopen.79531

Abstract

An investigation was carried out to determine the effect of nodular cast iron (NCI), nickel aluminum bronze (NAB), and Monel 400 microstructures on their cavitation erosion behavior in natural seawater. The cavitation tests were conducted using cavitation-induced facility at a frequency of 20 kHz on detached specimens. Morphological examinations by the scanning electron microscopy (SEM) on cavitated specimen indicated that the surfaces of NCI, NAB, and Monel 400 became very rough with large-size cavity pits. Localized material removal on the NCI surface was due to ductile tearing and brittle modes of failure and that for NAB and Monel 400 was due to grain boundary attack and micro-galvanic activities between the different phases of these two alloys. It was determined that the mechanical action of the collapsing air bubbles on the surfaces of the three alloys was the main cause of metal loss.

Keywords: cast iron, copper-based alloys, nickel-based alloys, mechanical factors

1. Introduction

The physical, chemical, mechanical, and corrosion properties of any metal or alloy highly depend on its microstructure. Based on this concept, alloy manufacturers develop specific materials to withstand aggressive and corrosive operating environments.

This study is relating the consequence of nodular cast iron (NCI), nickel-aluminum bronze (NAB), and Monel 400 microstructures to their cavitation erosion behavior, which were studied. This study is summarizing how the cavitation action is affecting the way metal loss is

occurring on alloy surfaces using seawater through time-lapse imaging as recorded by the scanning electron microscopy (SEM). It is not by any means the purpose of this section to provide an exhaustive cavitation analysis for a big list of available alloys in the market but to only focus on the three alloy microstructures mentioned above. Therefore, the main objectives of this chapter are to consider how these three alloys react and to summarize the role of materials properties with respect to cavitation erosion in seawater.

Cavitation erosion phenomenon is very complicated, and materials having different properties will react in different ways [1–4]. The main mechanism of a material's reaction to attack centers around mechanical stressing seems clear from available information. Cavity collapse will cause typical stresses at the material surface. Shear stresses within the material which arise from the nonuniformity of the normal pressure caused by the cavitation action can lead to plastic deformation [4].

2. Experimental

2.1. Apparatus

The ultrasonically induced cavitation technique used is made of a solid-state generator and a piezoceramic transducer which is designed to resonate at a frequency of 20 kHz at amplitude of 25 μm [5]. The transducer transmits the energy to the specimen tip through a velocity

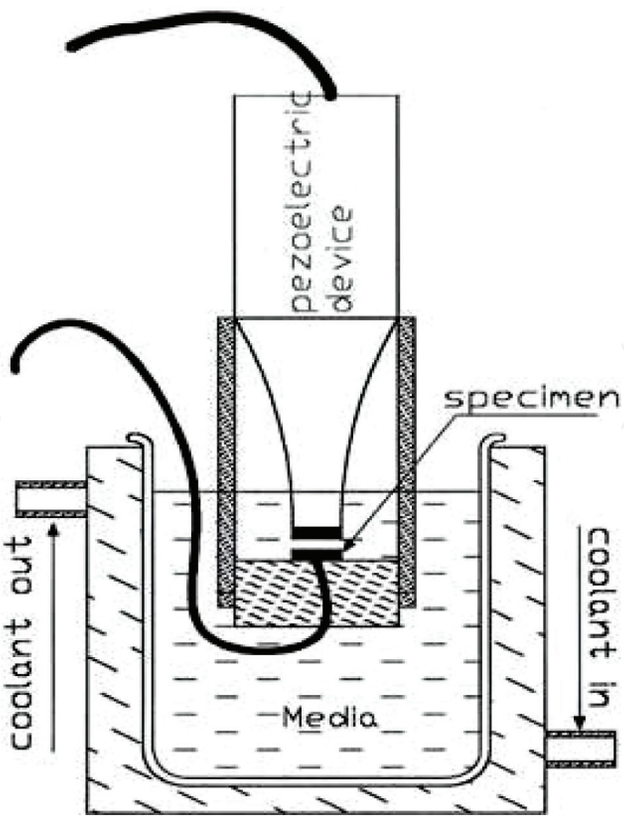

Figure 1. Schematic of vibratory cavitation test apparatus.

Parameter	Concentration (ppm ± SD)	Parameter	Concentration (ppm ± SD)
Sodium	12,300 ± 20	Bicarbonate	185 ± 18
Magnesium	1700 ± 150	Carbonate	14 ± 8
Potassium	470 ± 20	Total hydrocarbon	0.204
Calcium	570 ± 45	TDS	47,000 ± 2000
Chloride	24,000 ± 700	pH	8.2 ± 0.1
Sulfate	3400 ± 300		

Table 1. Chemical composition of Arabian Gulf seawater (Doha plant).

transformer, otherwise known as a horn. The main purpose of the velocity transformer is to increase the amplitude from that at the transducer face to the amplitude required at the specimen tip. The alloy samples were fixed using a special holder and being 0.125 cm way from the vibrating horn. Sample's surface area in these experiments was kept at 1 cm^2. The testing medium is Gulf seawater with high salinity (47,000 TDS) and was kept in special glass containers cooled with a water bath and maintained at 25 ± 1°C (**Figure 1**). **Table 1** shows the constituents of the testing medium.

2.2. Materials

The chemical composition of NCI consisted of 3.54 C, 2.26 Si, 0.40 Mn, 0.05 P, and the rest Fe. The microstructure of NCI after polishing and etching in 4% nital solution consisted of spheroidal graphite in a ferrite matrix. NAB specimen composition in weight percent was found to be 80 Cu, 9 Al, 4.9 Fe, 4.9 Ni, and 1.2 Mn. The percent (%) chemical composition of the UNS N04400 alloy includes 63.0 Ni, 28.0–34.0 Cu, 2.5 Fe, 2.0 Mn, 0.3 C, 0.024 S, 0.05 C, and 0.5 Si.

ASTM G32-G92 standard was followed for the preparation of all tested samples in terms of dimensions and surface preparation which then were etched before testing. Etching was made for all samples in order to be able to follow the mode of attack for the different constituent alloy's phases through time-lapse scanning electron microscopy SEM images.

3. Results

3.1. NCI assessment of surface damage

Metallographic examination of polished and etched NCI specimen revealed the structure of nodular cast iron of ferritic matrix. During the very early stages of cavitation testing in seawater, there was no damage observed on NCI sample surfaces. Micro-galvanic activity was detected at the graphite nodule and the ferrite matrix after 30 s of cavitation. This micro-galvanic activity allows the ferrite matrix to dissolve for being anodic to the graphite nodule, which is cathodic. Therefore, the first attacked area was the graphite/ferrite interface. SEM examinations of cavitated specimens for different periods of time were carried out to determine the morphology of cavitation damage as shown in **Figure 2**. After 15 min of cavitation testing in seawater, localized areas suffered from surface damage: some graphite nodules were

partially fragmented (**Figure 2a**), and others were totally removed (**Figure 2b**). After 30 min of cavitation (**Figure 2c**), total removal of the graphite nodules was dominant. The average size of these cavities was generally 30–80 μm in diameter which to a certain extent similar to that of the graphite nodules. The presence of other micro-cavities (2 μm) in the matrix

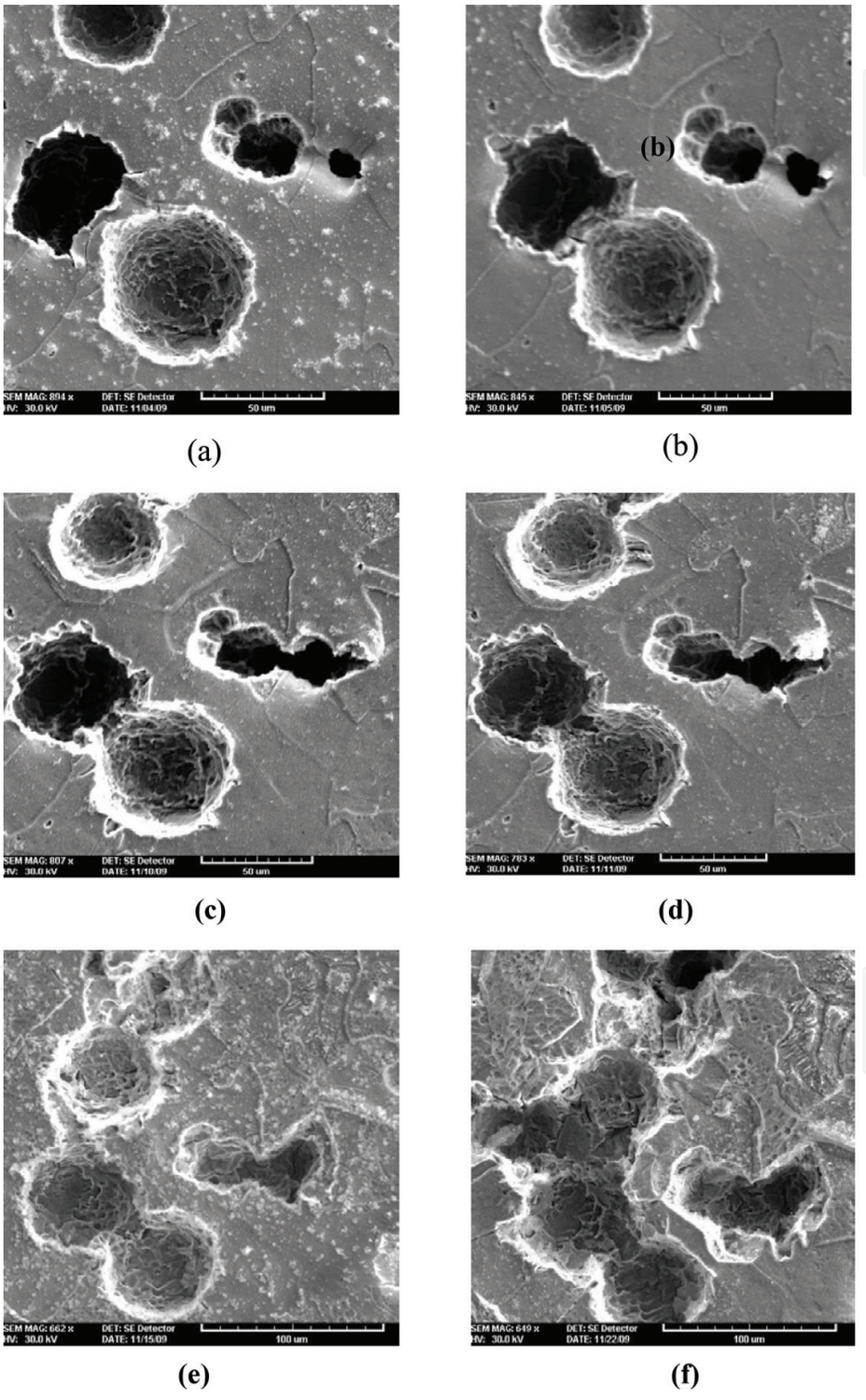

Figure 2. SEM micrographs of the gradual destruction and fragmentation of graphite nodules and plastic deformation of the ferrite matrix as a function of cavitation testing in seawater: (a) 15 min, (b) 20 min, (c) 30 min, (d) 70 min, (e) 120 min, and (f) 240 min.

http://dx.doi.org/10.5772/intechopen.79531

of this alloy that are not related to the removal of the graphite nodules was also observed. Surface deformations with an increasing number of cavities and pitting were observed on the attacked areas of the specimen after 70 min of testing (**Figure 2d**). The cavitation damage has extended to other areas on the alloy's sample causing the formation of large cavities after 120 min (**Figure 2e**). After 240 min of cavitation (**Figure 2f**), the ductile removal of material in the ferrite matrix leads to the coalescence of these pits with time forming deep craters on the surface of NCI specimens.

The cavitation action has led to the fragmentation of a graphitic nodule and partial removal of another. In addition to the cavity pit that formed as a result of the removal of graphite nodule, several micropits were also formed on the surface of the ferrite matrix.

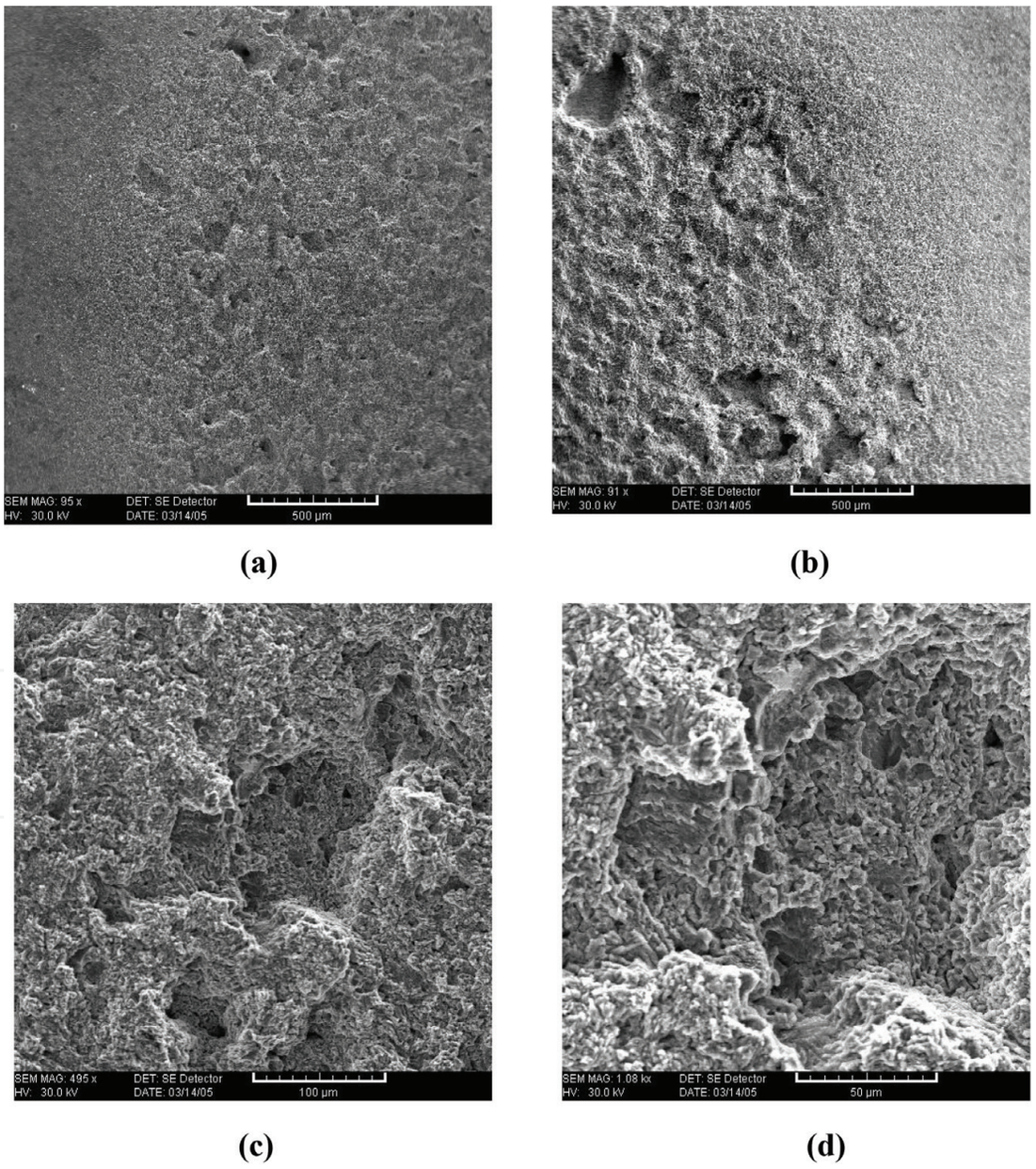

Figure 3. SEM micrographs of the surface of NAB after cavitation testing in seawater for various lengths of time: (a) 3 h, (b) 13 h, (c) 25 h, and (d) 40 h.

3.2. NAB assessment of surface damage

In order to understand the performance of NAB against cavitation erosion, it is of interest to understand its complex microstructure. There are many constituent phases that make up the microstructure of NAB which includes the following: α phase which is a *fcc* copper-rich solid solution, eutectoid phases of "β phase" or retain β, and four intermetallic κ phases designated as κ_I, κ_{II}, κ_{III}, and κ_{VI} [6–9]. The κ_I, κ_{II}, and κ_{IV} phases are all iron-rich precipitates based on the structure of Ni-Al [9]. The κ_{II} and κ_{IV} precipitates were found to be 10 μm in size and <0.5 μm in thickness, respectively. The microstructure also contains a precipitate free zone at the α grain periphery.

After 3 h of cavitation testing, the NAB surface became a bit rough as shown by SEM micrographs in **Figure 3a**. The surface damage increased, and several micro-cavities were observed on NAB surface after 13 h of cavitation (**Figure 3b**).

The NAB surface contained large-size cavities after 25 h of testing (**Figure 3c**). Severe surface roughness was observed, and the amount of cavities has increased after 40 h of testing period (**Figure 3d**). Later on and after 40 h of cavitation testing, ductile tearing and grain boundary attack were detected.

When NAB-polished samples were immersed in stagnant seawater for 48 h, examinations by SEM indicated that the α phase was preferentially attacked at the α/κ_{IV} interfaces (**Figure 4a** and **b**).

3.3. Monel 400 assessment of surface damage

Figure 5a–d shows SEM micrographs of a standard specimen of Monel 400 before and after cavitation testing revealing its solid solution binary structure. **Figure 5a** shows the microstructure of this alloy in the as-received solution heat-treated condition. The microstructure

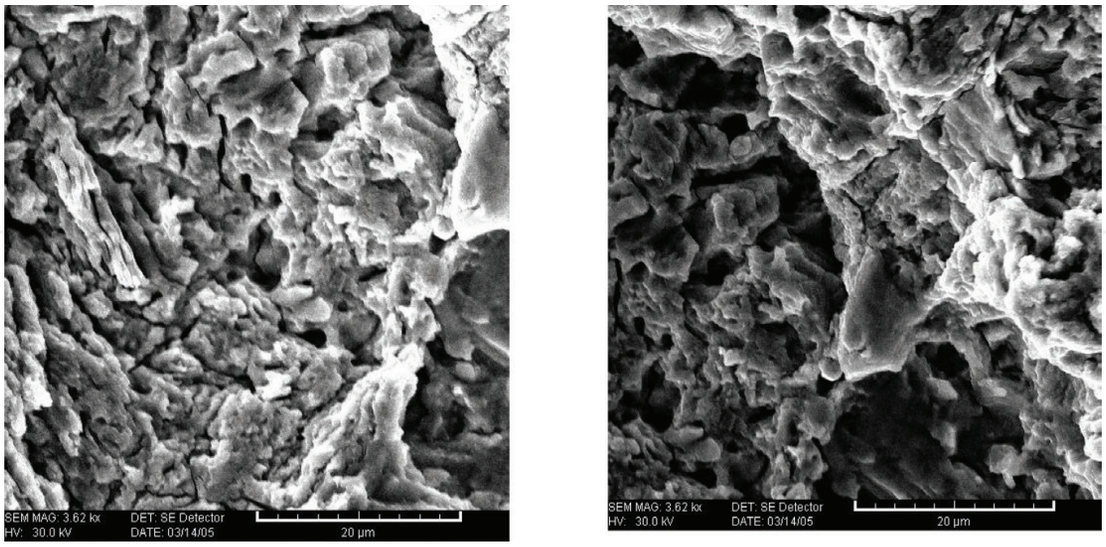

Figure 4. SEM micrographs of NAB after exposure to quiescent seawater for 48 h, showing preferential attack of the α phase at the α/κ_{III} interfaces. The precipitate free zone did not suffer from corrosion attack (3620×).

http://dx.doi.org/10.5772/intechopen.79531

consists essentially of a single face-centered cubic (FCC) phase with some of annealing twins. The grain size varied from 25 to 100 μm in **Figure 5a**.

Small second-phase particles of possibly manganese sulfide and silicon carbide are also present in the microstructure of **Figure 5a**. **Figure 5b–d** shows SEM micrographs of the same region of this specimen after 0.66, 1.10, and 1.42 h of cavitation in seawater, respectively. Minimal surface attack was observed after 0.66 h of cavitation. However, after 1.10–1.42 h of cavitation, attack is visible along grain boundaries, twins, and plastic deformation of the matrix.

The presence of cavities and ductile tearing is readily explainable in terms of the known devastating effects of cavitation.

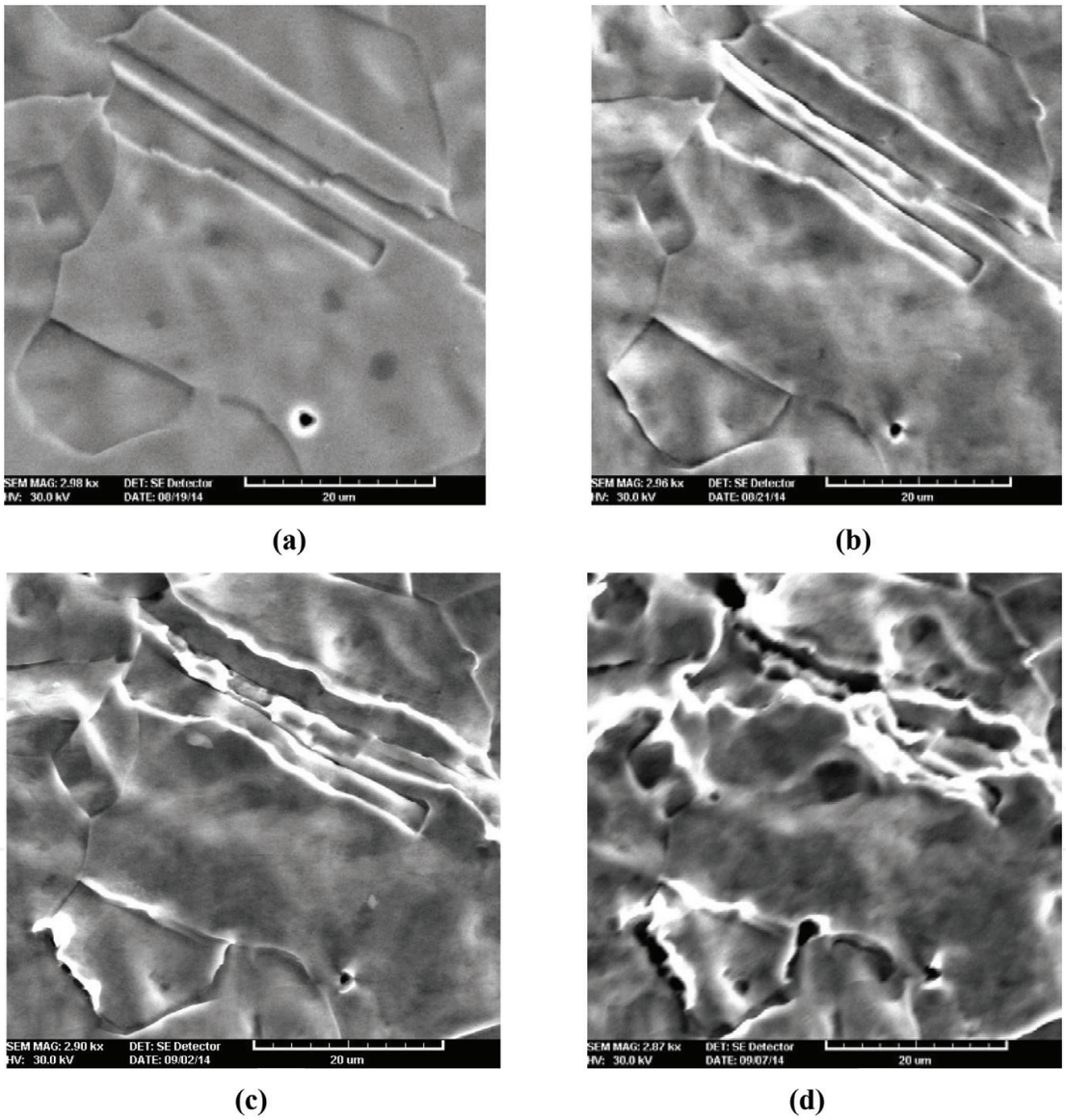

Figure 5. SEM micrograph of the surface of UNS N04400 alloy at high magnifications after (a) 0.0 h, (b) 0.66 h, (c) 1.10 h, and (d) 1.42 h of cavitation testing in seawater at 25°C showing the damage at grain boundaries, annealing twins, and the matrix.

4. Discussion

4.1. NCI

In the early stages of NCI cavitation testing, the damage appeared as fragmentation of some graphite nodules and the total removal of others leaving surface cavities. The cavitation damage of nodular cast iron is initiated both at the ferrite matrix and graphite nodules [10–13]. The large removal rate of material from the NCI surface was attributed to the fragmentation of graphite nodules for being brittle and ductile tearing of the ferrite matrix and brittle in areas of matrix where a cluster of cavities existed.

The presence of subsurface cracks deep into the ferrite matrix is possible due to little ductility and the brittle nature of NCI, which is exhibited during the vibratory cavitation conditions. The mechanical impact of the cavitation action on the surface of a body-centered cubic (BCC) metal or alloy such as NCI would lead to a transition from ductile to brittle behavior causing plastic deformation and metal loss [14–16].

4.2. NAB

Figure 3 shows that the cavitation action on the surface of NAB sample has created large-size cavities causing the surface to be rough. Grain boundary attack and ductile tearing were also detected under stagnant condition. NAB surface damage and metal loss can also be attributed to surface and interfacial defects as well as the electrochemical dissolution of the matrix along the intermetallic particle interfaces.

Microcracks (5–10 μm) were detected at the α phase and right next to κ precipitates as shown in **Figure 4**. It is believed [6–9] that the intermetallic κ precipitates are known to be cathodic to the α matrix, thus causing the areas adjacent to them to dissolve electrochemically when exposed to seawater. It is only the mechanical action of the collapsing air bubbles of the cavitation process that plays a major role in the removal of the κ precipitates (**Figure 4**). Therefore, metal loss of NAB under cavitation conditions in seawater may be attributed to mechanical and galvanic factors as was reported by other authors [13, 17–19].

4.3. Monel 400

The morphological investigation revealed that corrosion initiated locally at grain boundaries and twin lines of Monel 400 alloy. It is believed that both the mechanical action of the attacking vapor bubbles and the micro-galvanic activity between the matrix and the manganese sulfide and silicon carbide second-phase particles lead to metal loss from the FCC matrix. The cyclic mechanical contact of the bubbles on the surface of this alloy has led to slight ductile plastic deformation of its FCC matrix.

Therefore, the cavitation-corrosion resistance of the Monel 400 alloy can be due to its inherent matrix corrosion resistance and its high strength. It is also believed that the slight plastic deformation of the matrix (grains) is probably due to cyclic stresses [19–25].

5. Conclusions

1. The cavitation erosion of NCI, NAB, and Monel 400 alloys under ultrasonically induced cavitation testing in seawater was attributed mainly to the mechanical factors.
2. Graphite nodule fragmentation, ductile tearing, and micro-galvanic activities at graphite/ferrite interface are believed to be the main mechanisms of metal loss of NCI in seawater.
3. For NAB, α phase was selectively attacked at the interfaces with the intermetallic κ precipitates in quiescent seawater. The κ precipitates and the precipitate free zones did not suffer from corrosion. Selective phase corrosion and cavitation stresses were considered to be the causes of cracking.
4. The formation of slightly rough surfaces for this alloy with attacks along grain boundaries, annealing twins, as well as plastically deformed matrix regions. Corrosion of Monel 400 alloy mainly initiated in and around the grain boundaries, annealing twins, and second-phase particles leading to metal loss.

Acknowledgements

The authors would like to thank Kuwait Foundation for the Advancement of Science (KFAS) for its partial financial support of this work.

Author details

Abdulhameed Al-Hashem*, Abdulmajeed Abdullah and Wafa Riad

*Address all correspondence to: ahashem@kisr.edu.kw

Petroleum Research Center, Kuwait Institute for Scientific Research, Safat, Kuwait

References

[1] McCaul C. An advanced cavitation resistant austenitic stainless steel for pumps. Corrosion'96, Paper No. 415. Houston, TX: NACE International; 1996

[2] Marques PV, Trevisan RE. An SEM-based method for the evaluation of the cavitation erosion behaviour of materials. Materials Characterization. 1998;**41**:193-200

[3] Kim K-H, Chahine G, Franc J-P, Karimi A, editors. Advanced Experimental and Numerical Techniques for Cavitation Erosion Prediction. Dordrecht: Springer Publishing; 2014

[4] Al-Hashem A, Carew J, Abdullah A, Al-Mazeedi H, Riad W. Effect of ultrasonically induced cavitation on the corrosion behaviour of NAB alloy, microstructural aspects. Journal of the Faculty of Science, UAE University. 1994;**6**(10):207-217

[5] Designation: G 32-09: Standard Test Method for Cavitation Erosion Using Vibratory Apparatus. Annual Book of ASTM Standards (2010), Section 3: Metals test method and analytical procedures. Vol. 03.02. West Conshohocken. pp. 94-109

[6] Berchiche N, Franc JP, Michel JM. A cavitation erosion model for ductile materials. Journal of Fluids Engineering. 2002;**124**(3):601-606

[7] Song QN, Xu N, Gu W, Bao YF, Wei CY, Ni FS, Zheng YG, Ni DR, Qiao YX. Investigation on the corrosion and cavitation erosion behaviors of the cast and friction stir processed Ni-Al bronze in sulfide-containing chloride solution. International Journal of Electrochemical Science. 2017;**12**:10616-10632

[8] Franc J-P, Michel J-M. Fundamentals of cavitation. In: Morean R, editor. Fliud Mechanics and its Applications. Dordrecht: Springer; 2004

[9] Hasan F, Iqbal J, Ridley N. Microstructure of as-cast aluminum bronze containing iron. Materials Science and Technology. 1985;**1**:312

[10] Franc J-P. Incubation time and cavitation erosion rate of work-hardening materials. Journal of Fluids Engineering. 2009;**131**(2):021303

[11] Carnelli D, Karimi A, Franc J-P. Application of spherical nanoindentations to determine the pressure of cavitation impacts from pitting tests. Journal of Materials Research. 2012;**27**(1):91-99

[12] Loriner GW, Hasan F, Iqbal J, Ridley N. Observation of microstructure and corrosion behaviour of some aluminum bronzes. British Corrosion Journal. 1986;**21**(4):244-247

[13] Gouda VK, Al-hashem AH, Abdullah AM, Riad WT. Effect of ultrasonically induced cavitation on the behavior of nodular cast iron in seawater. British Corrosion Journal. 1991;**26**(2):109

[14] Eskilsson C, Bensow RE. Estimation of cavitation rrosion intensity using CFD: Numerical comparison of three different methods. In: Paper Presented at the Fourth International Symposium on Marine Propulsors, Smp'15; Austin, Texas, USA; 2015

[15] Steller J, Knella A, Koronowicz J, Janicki W. Towards quantitative assessment of materials resistance to cavitation erosion. Wear. 2005;**258**(1-4):604-613

[16] Al-Hashem A, Tarish H, Akbar A, Carew J. Cavitation corrosion behavior of copper- and nickel based alloys in seawater. In: Presented at the 11th Middle East Corrosion Conference; 26th February-1st March 2006; Manama, Kingdom of Bahrain

[17] Al-Hashem A, Tarish H, Akbar A. Cavitation corrosion behavior of carbon steel, Al-Bronze and Cobalt-based alloys in seawater. In: Corrosion 2007, Paper # 07253. Nashville, Tennessee: NACE International; 2007

[18] Al-Hashem A, Tarish H, Carew J. The effect of ultrasonically induced cavitation conditions on the behavior of copper and nickel based alloys in seawater. In: Corrosion/06, Paper No. 299. Houston, TX: NACE International; 2006

[19] Al-Hashem A, Tarish H, Tanoli N. The effect of ultrasonically induced cavitation conditions on the behavior of Ni-resist cast alloys in seawater. In: Corrosion/10, Paper No. 10392. Houston, TX: NACE International; 2010

[20] Al-Hashem A, Tarish H, Tanoli N. The cavitation corrosion behavior of UNS G10950 alloy in seawater. In: Corrosion 2013, Paper # 2201. Orlando, Florida: NACE-International; 2013

[21] Al-Hashem A, Tarish H, Tanoli N. The ultrasonically induced cavitation corrosion of UNS N08825 in seawater. In: Corrosion/2014, Paper # 3803. San Antonio, Texas: NACE-International; 2014

[22] Hobbs JM. Erosion by Cavitation or Impingement, STP 408. Philadelphia PA: ASM; 1967. p. 159

[23] McGuiness T, Thijuvengadam A. Erosion Wear and Interfaces with Corrosion, STP 567. Philadelphia, PA: ASTM; 1974. p. 30

[24] Auret JG, Damm OFR, Wright GJ, Robinson FPA. Influence of cathodic and andodic currents on cavitation erosion. Corrosion. 1993;**49**(11):910

[25] Farhangi H, Armstromg RW, Regnault WF. Transmission electron microscopy detection of cyclic-deformation-induced f.c.c.-to-h.c.p. Transformation in a cobalt-based prosthetic device material. Materials Science and Engineering. 1989;**114**:25-28

IntechOpen